Supporting Information

For

Photo-Rechargeable Zinc-Ion Capacitor using 2D Graphitic Carbon Nitride

Buddha Deka Boruah[1,*], Angus Mathieson[1,2], Bo Wen[1,2], Changshin Jo[1], Felix Deschler[3], Michael De Volder[1,*]

[1] Institute for Manufacturing, Department of Engineering, University of Cambridge, Cambridge CB3 0FS, United Kingdom
[2] Cambridge Graphene Centre, University of Cambridge, Cambridge CB3 0FA, United Kingdom
[3] Walter Schottky Institut, Fakultät für Physik, Technische Universität München, Am Coulombwall 4, 85748 Garching bei München

* Corresponding authors. E-mail: bd411@cam.ac.uk
E-mail: mfld2@cam.ac.uk

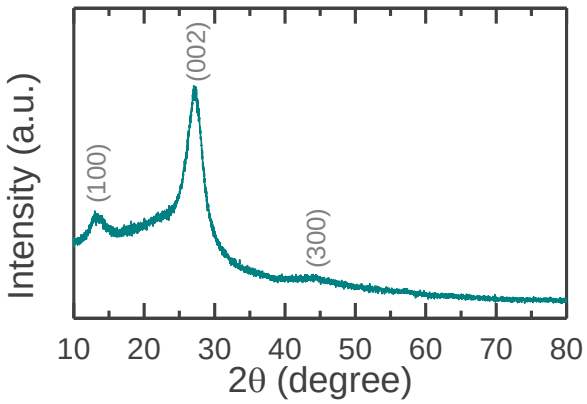

Figure S1. *XRD pattern of as-synthesized g-C_3N_4.*

Figure S1 shows the XRD pattern of the as-prepared g-C_3N_4, where the attributed two distinct diffraction peaks at around 2θ ~ 13° (100) and 27° (002) along with an additional week diffraction peak at 2θ ~ 44.3° (300) confirm the layers of triazine units with a 3D A-B stacking, which belongs to hexagonal unit cell and space group of $P\bar{6}m2$ with lattice parameters of a = b = 4.7420 Å, c = 6.7205 Å, α = β = 90°, γ = 120°.[1] The characteristic diffraction peak corresponds to (100) planes observed because of the interlayer structural packing, whereas the peak of (002) originates because of interplanar stacking of aromatic systems of g-C_3N_4.[2]

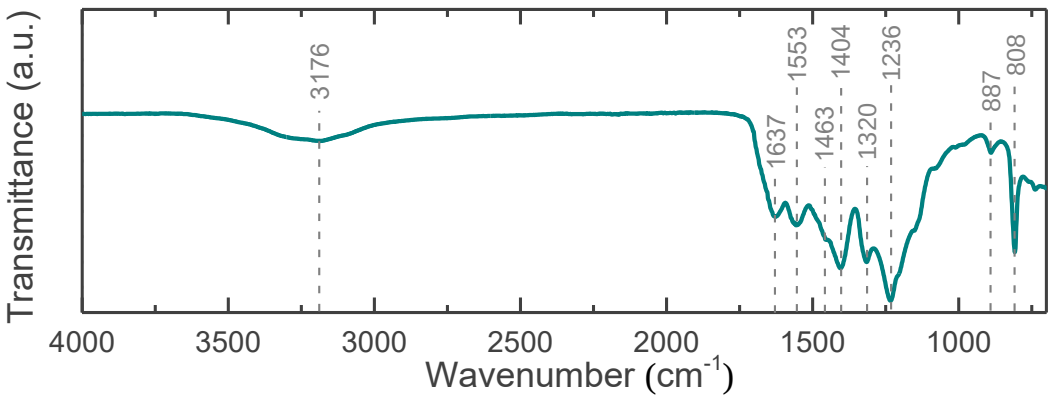

Figure S2. *FTIR spectrum of g-C_3N_4.*

Figure S2 shows the FTIR spectrum of the g-C_3N_4, where the characteristic peak at around 808 cm^{-1} is attributed because of the breathing vibration of triazine ring.[3,4] The peak at ~ 887 cm^{-1} represents the deformation mode of cross-linked heptazine. The characteristic peak at ~ 1637 cm^{-1} is assigned to the C=N stretching vibration mode, whereas the additional characteristic peaks at 1236 cm^{-1}, 1320 cm^{-1}, 1404 cm^{-1}, 1463 cm^{-1}, and 1553 cm^{-1} are attributed to stretching modes of C-N heterocycles.[5] In addition, a characteristic broad peak centered at around 3176 cm^{-1} corresponds to the N-H bond stretching mode.[6]

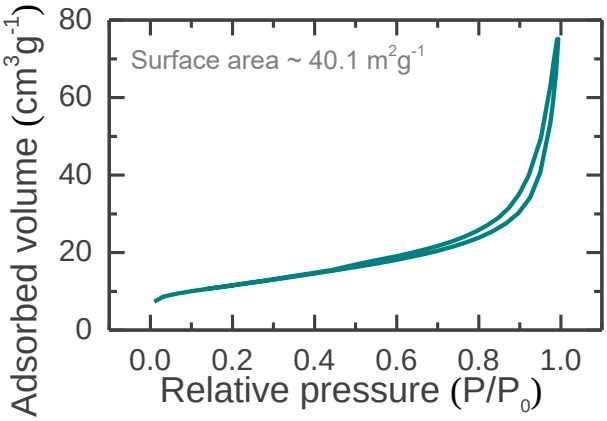

Figure S3. *BET N_2 adsorption/desorption isotherms of g-C_3N_4.*

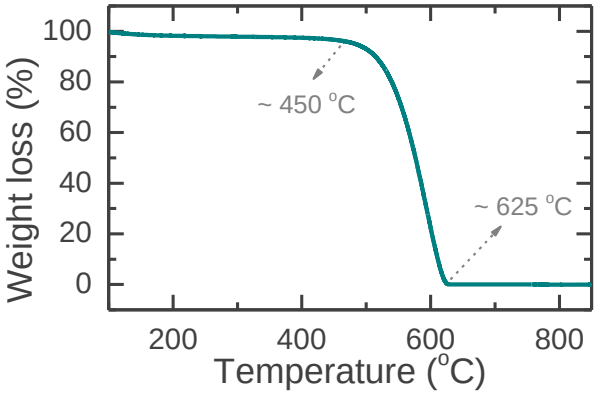

Figure S4. *TGA curve of as-prepared g-C_3N_4.*

Figure S3 shows the BET N_2 adsorption/desorption isotherms of g-C_3N_4 corresponds to the surface area of ~ 40.1 m^2/g. The TGA curve of the g-C_3N_4 is shown in **Figure S4**, where a rapid decay of TGA curve is attributed in the temperature range from ~ 450 ℃ to ~ 625 ℃ denoting the thermal decomposition temperature range of g-C_3N_4.

GO and rGO samples were characterized by SEM, XRD and Raman. **Figure S5a,b** show the SEM images of GO and rGO, where more porous 2D sheets are observed in the rGO sample as compared to pristine GO. The evidence of the reduction of GO can be confirmed from the XRD patterns (**Figure S5c**), where a strong diffraction peak at $2\theta \sim 10.6^o$ corresponds to (001) diffraction planes was observed in GO which is vanished in rGO. Moreover, a new distinct peak at around $2\theta \sim 24.2^o$ (002) attributed is attributed in rGO. In addition, the defect states in

rGO was slightly increased because of increase in the surface related defect states during reduction process (**Figure S5d**, Raman spectra).

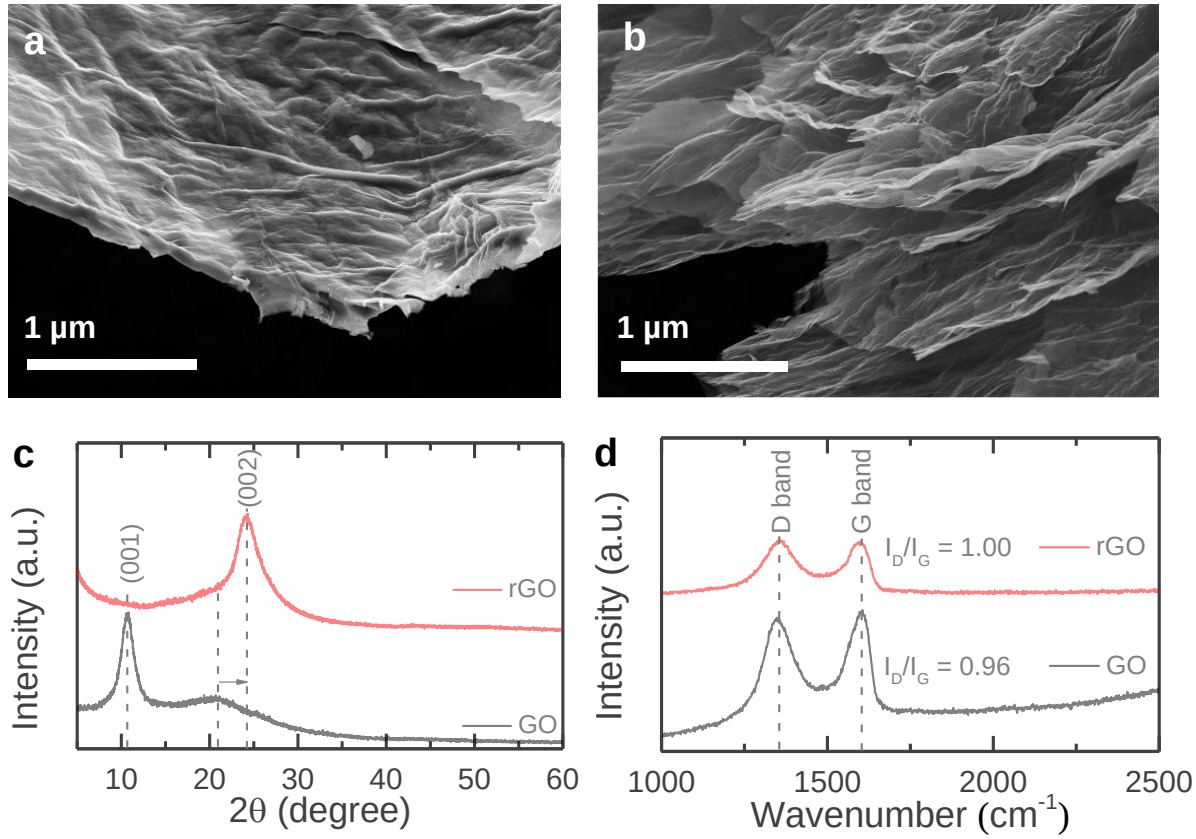

Figure S5. *(a,b) SEM images of GO and rGO. (c,d) XRD patterns and Raman spectra of GO and rGO.*

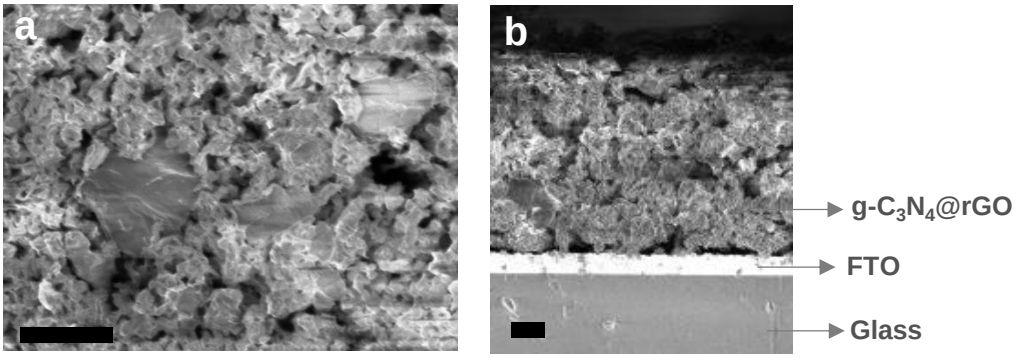

Figure S6. *(a) Top-view and (b) cross-section SEM images of the photo-cathode. Scale ~ 1µm.*

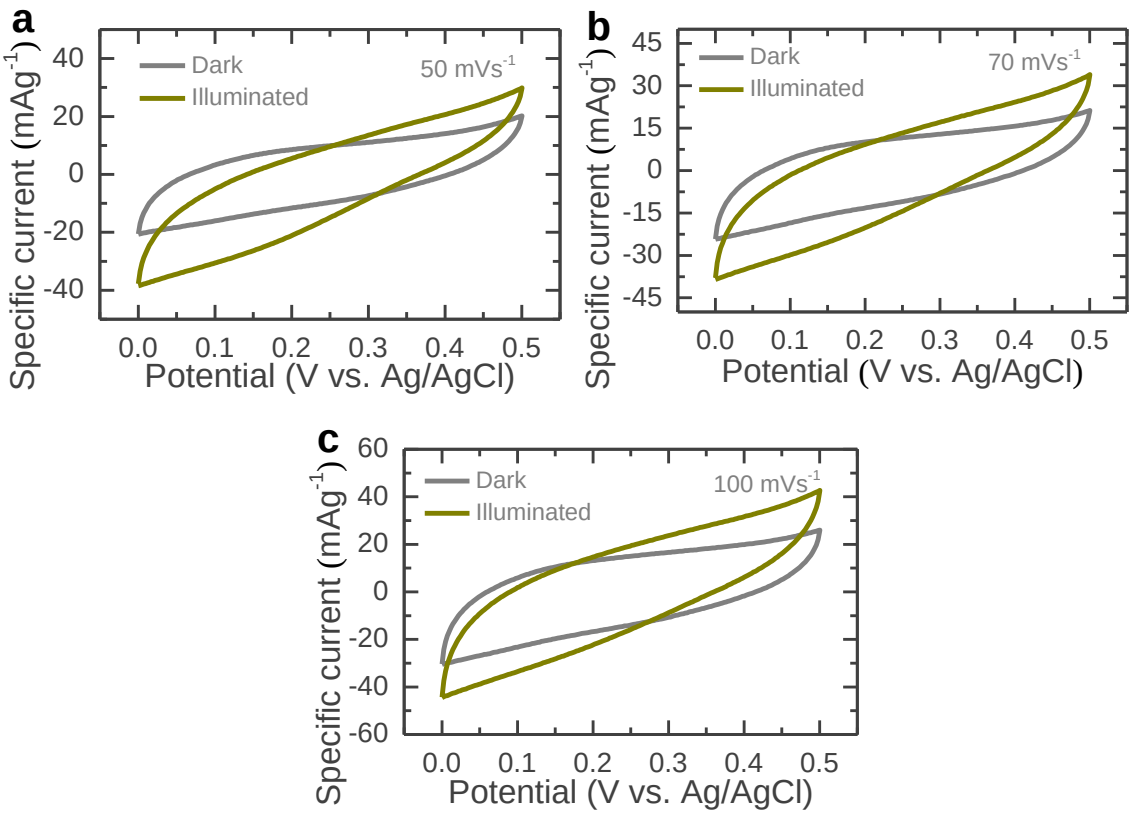

Figure S7. *CV responses of g-C_3N_4@rGO/FTO electrode at scans of (a) 50 mVs^{-1}, (b) 70 mVs^{-1} and (c) 100 mVs^{-1} in dark and illuminated (λ ~ 420 nm, intensity ~ 50 $mWcm^{-2}$) conditions.*

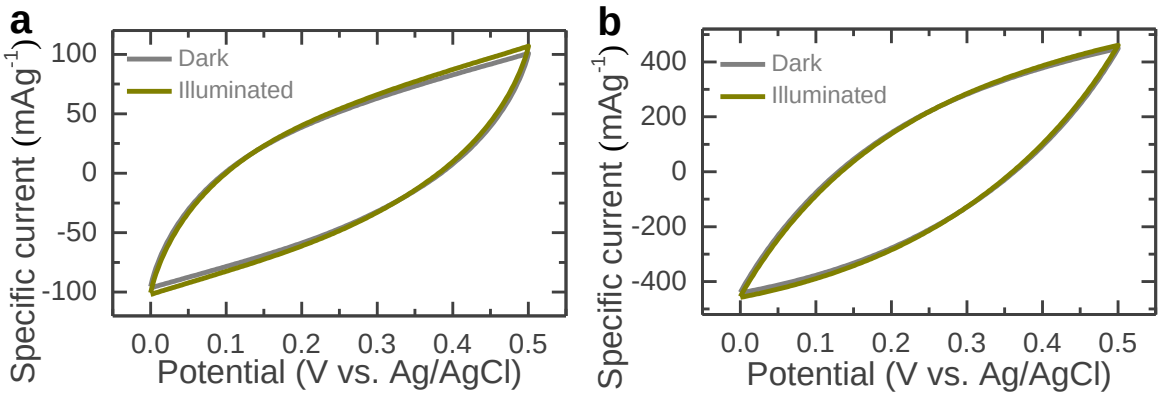

Figure S8. *CV profiles of (a) rGO/FTO and (b) activated carbon/FTO electrodes recorded in dark and illuminated (λ ~ 420 nm, intensity ~ 50 mWcm^{-2}) conditions at same scan rate of 50 mVs^{-1}.*

Figure S8 shows the CV profiles of rGO/FTO electrode (**Figure S8a**) and activated carbon/FTO electrode (**Figure S8b**) acquired by three-electrode testing in dark and illuminated (λ ~ 420 nm, intensity ~ 50 mWcm^{-2}). Interestingly, negligible increase in the area under CV of rGO/FTO electrode is observed because of the relatively weak light sensitive response of rGO. However, as expected no change in the area under CV plot of the activated carbon/FTO electrode is observed (see **Figure S8b)**.

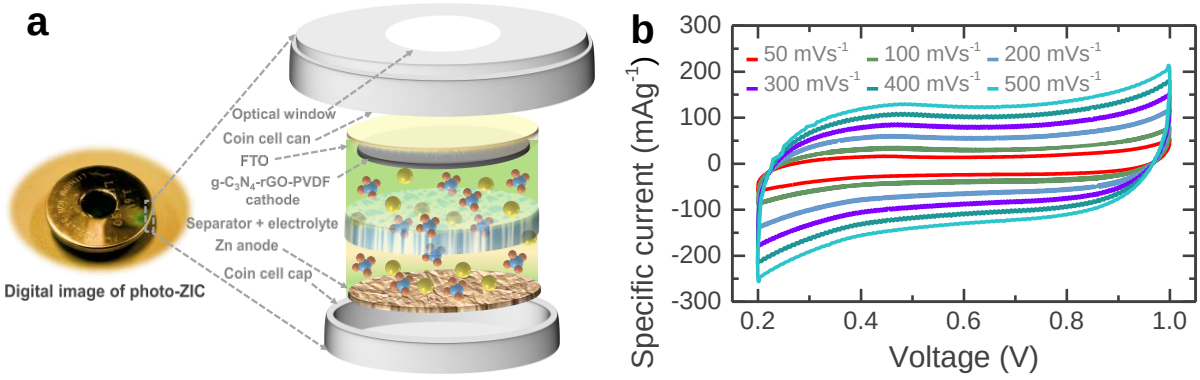

Figure S9. *(a) Digital photograph (left) and schematic representation (right) of an optical coin cell (CR2450) with an optical window of ~ 8 mm diameter designed for Photo-ZIC devices. (b)*

CV responses of the Photo-ZIC at different scan rates of 50 mVs^{-1}, 100 mVs^{-1}, 200 mVs^{-1}, 300 mVs^{-1}, 400 mVs^{-1} and 500 mVs^{-1} in dark.

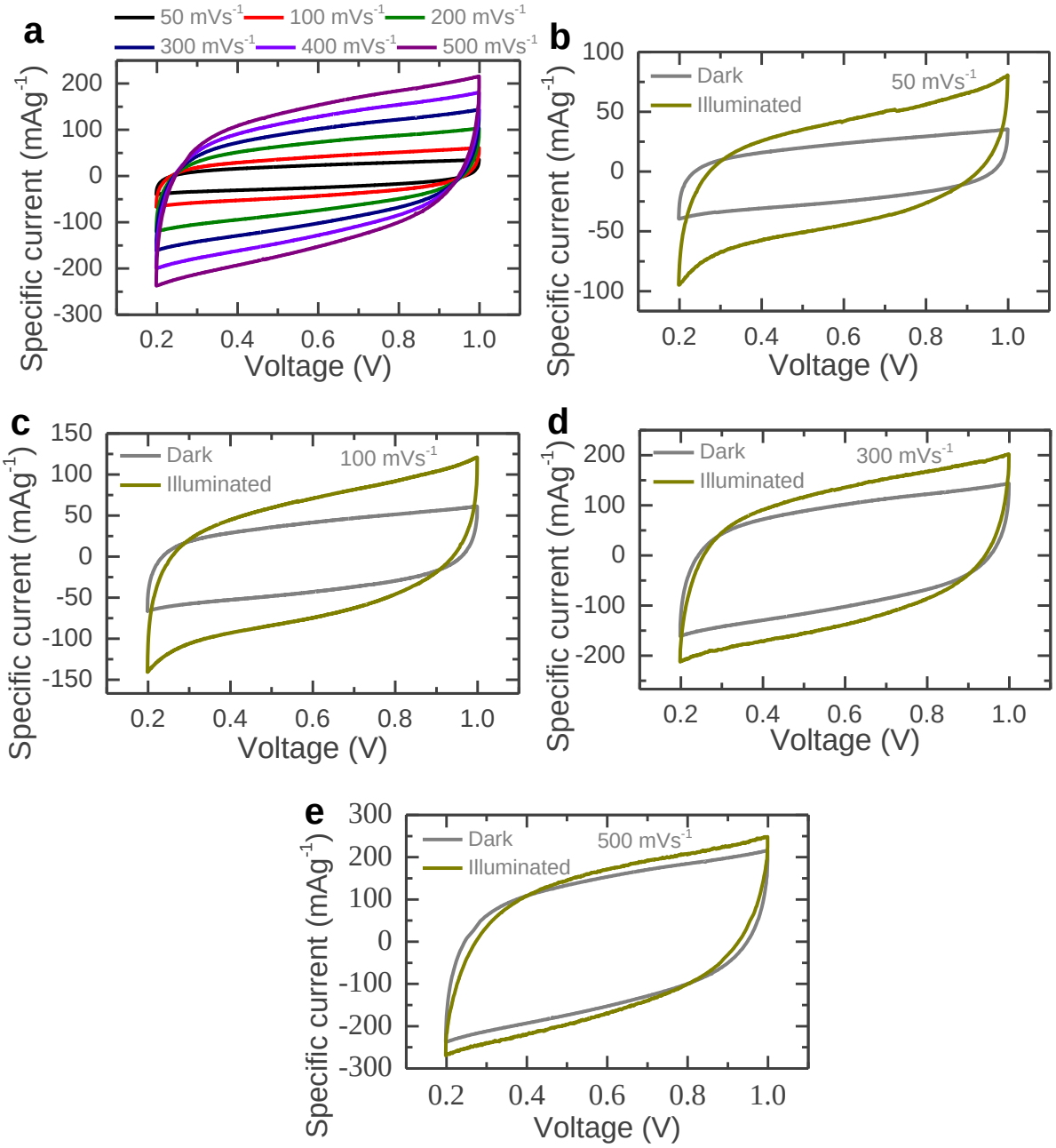

Figure S10. *(a) CV profiles (50 to 500 mVs^{-1}) of a Photo-ZIC in 1M $Zn(CF_3SO_3)_2$ aqueous electrolyte. Comparative CV studies of the photo-ZIC in 1M $Zn(CF_3SO_3)_2$ aqueous electrolyte at different scans of (b) 50 mVs^{-1}, (c) 100 mVs^{-1}, (d) 300 mVs^{-1} and (e) 500 mVs^{-1} in dark and illuminated ($\lambda \sim 420$ nm, intensity ~ 50 $mWcm^{-2}$) conditions.*

Figure S10a shows the CV profiles of the Photo-ZIC in 1M $Zn(CF_3SO_3)_2$ aqueous electrolyte at different scans (50 to 500 mVs^{-1}). Similarly, the photo-charging responses can be observed of the Photo-ZIC in $Zn(CF_3SO_3)_2$ aqueous electrolyte, which implies that $ZnSO_4$ or $Zn(CF_3SO_3)_2$ aqueous electrolytes can be used for the realization of photo-rechargeable ZIC based on the optically and electrochemically active g-C_3N_4 cathode. Comparative CV plots of the Photo-ZIC in 1M $Zn(CF_3SO_3)_2$ aqueous electrolyte at different scans of 50 mVs^{-1}, 100 mVs^{-1}, 300 mVs^{-1} and 500 mVs^{-1} in dark and illuminated conditions ($\lambda \sim 420$ nm, intensity ~ 50 $mWcm^{-2}$) show the clear enhancements of capacitive responses under light illumination as compared to dark (**Figure S10b-e)**.

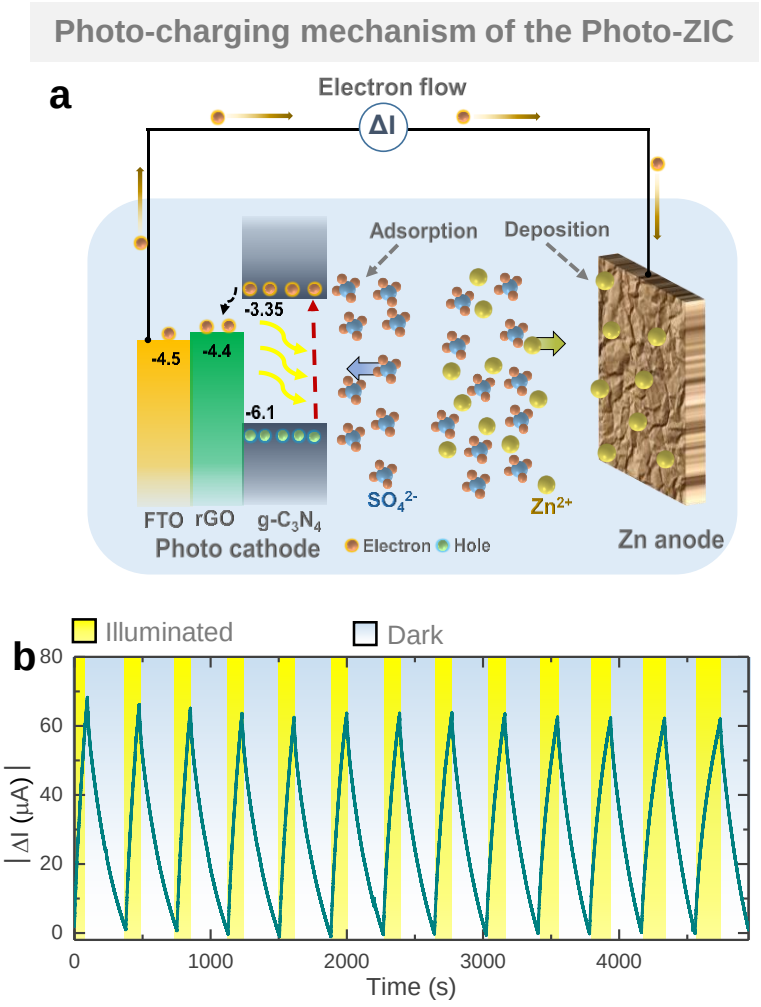

Figure S11. *(a) Energy level diagram of the Photo-ZIC demonstrating the participation of photogenerated electrons and holes for photo-charging under illumination. (b) Cyclic current*

response ($\Delta I = I_{light} - I_{dark}$; where I_{dark} and I_{light} are the currents in dark and illuminated conditions) of the Photo-ZIC in illuminated and dark conditions at 0 V applied voltage.

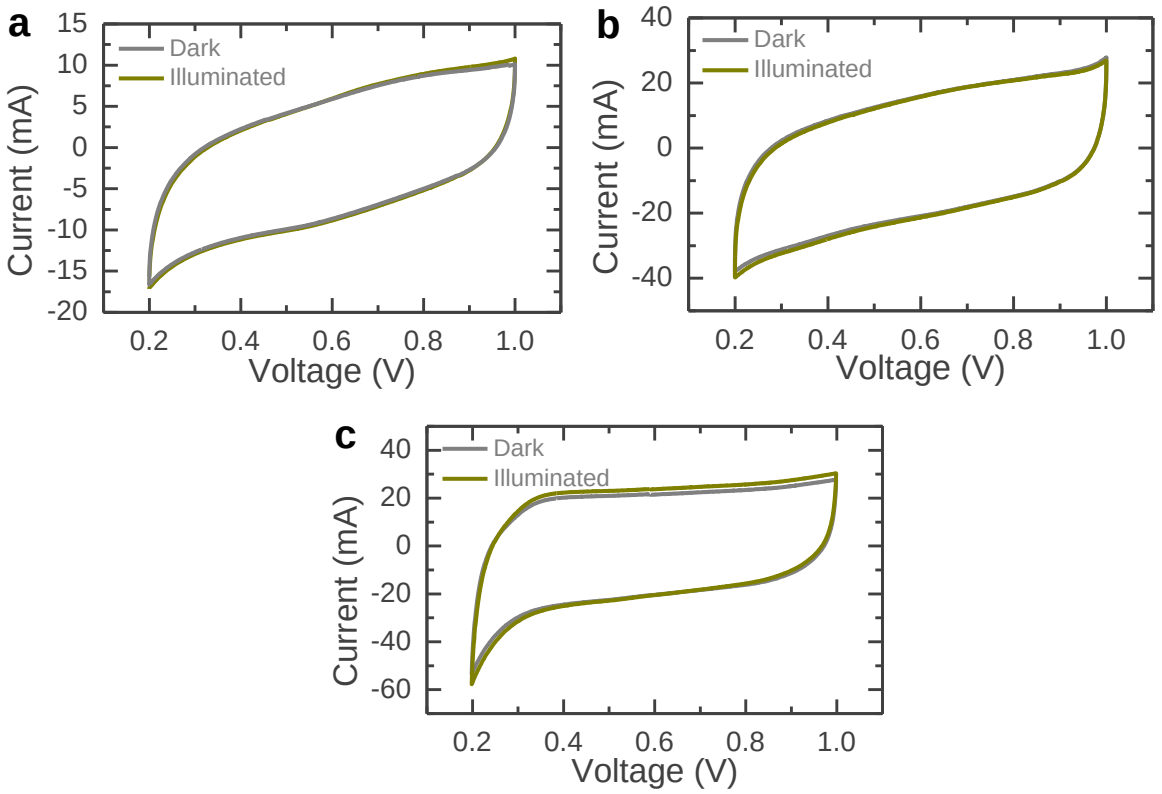

Figure S12. *CV curves of (a) rGO/FTO//Zn, (b) activated carbon/FTO//Zn and (c) g-C_3N_4@SuperP/FTO//Zn based ZICs in dark and illuminated (λ ~ 420 nm, intensities of ~ 50 mWcm^{-2}) conditions.*

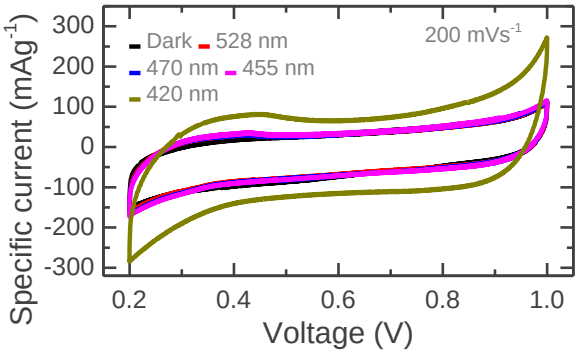

Figure S13. *CV responses in dark and different light illuminated conditions. Scan rate = 200 mVs^{-1}.*

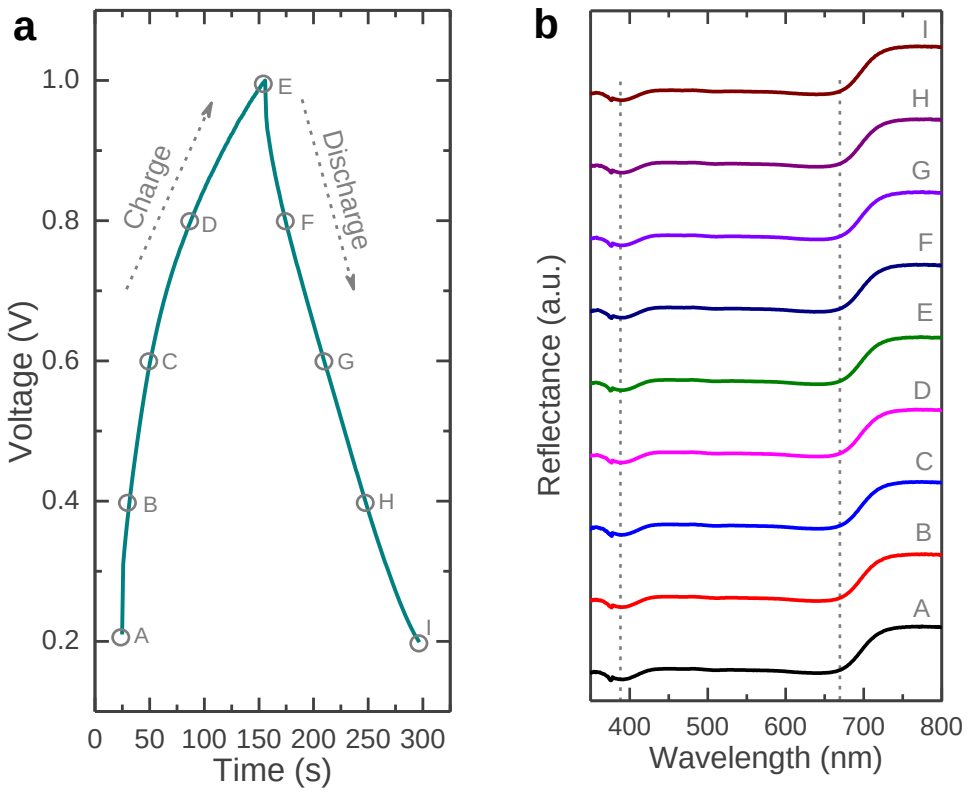

Figure S14. *In operando optical characterisation of the Photo-ZIC. (a) Galvanostatic charge-discharge profile and (b) reflectance spectra at different charge and discharge voltages.*

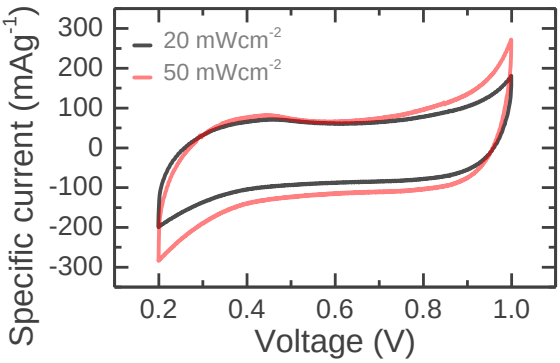

Figure S15. *Intensity dependence CV responses of the photo-ZIC at λ ~ 420 nm with intensities of ~ 20 mWcm^{-2} (black) and ~ 50 mWcm^{-2} (red).*

Table S1. Comparative voltage response and photo-charge conversion efficiency of the Photo-ZIC with previously reported photo-rechargeable supercapacitors (with externally integrated solar cells).

Photo-rechargeable Energy Storage Unit	Architecture	Voltage response	Photo-charge conversion efficiency
AC//AC SC and DSSC[7]	Integrated	460 mV	-
PEDOT//PEDOT SC and DSSC[8]	Integrated	690 mV	-
CNTs-TiO_2//CNTs-TiO_2 SC and DSSC[9]	Integrated	600 mV	1.5%
WO_3//WO_3 SC and PSC[10]	Integrated	680 mV	-
BC-PPy nanofibers//MWCNTs SC and PSC[11]	Integrated	710 mV	10
MWCNTs//MWCNTs SC and DSSC[12]	Integrated	650 mV	1.83%
TiO_2//MWCNTs SC and DSSC[13]	Integrated	630 mV	2.73%
TiO_2//TiO_2 SC and DSSC[14]	Integrated	610 mV	1.64%
PANI//PANI SC and DSSC[15]	Integrated	620 mV	2.12%
Porous Si//porous Si SC and DSSC[16]	Integrated	640 mV	2.1%
TiO_2//MWCNTs SC and polymer solar cell[17]	Integrated	400 mV	0.82%
PEDOT-carbon//PEDOT-carbon SC and PSC[18]	Integrated	710 mV	4.7%
Carbon//Carbon SC and PSC[19]	Integrated	910 mV	71%
CF@TiO_2@MoS_2//CF@TiO_2 @MoS_2 SC and DSSC[20]	Integrated	750 mV	1.8%
Carbon//Carbon SC and PSC[21]	Integrated	950 mV	7.1%
Photo-ZIC (This work)	**Single**	**850 mV**	**0.01%**

AC: Activated carbon, SC: Supercapacitor, DSSC: dye-sensitized solar cell, PSC: perovskite solar cell, MWCNTs: Multi-walled CNTs.

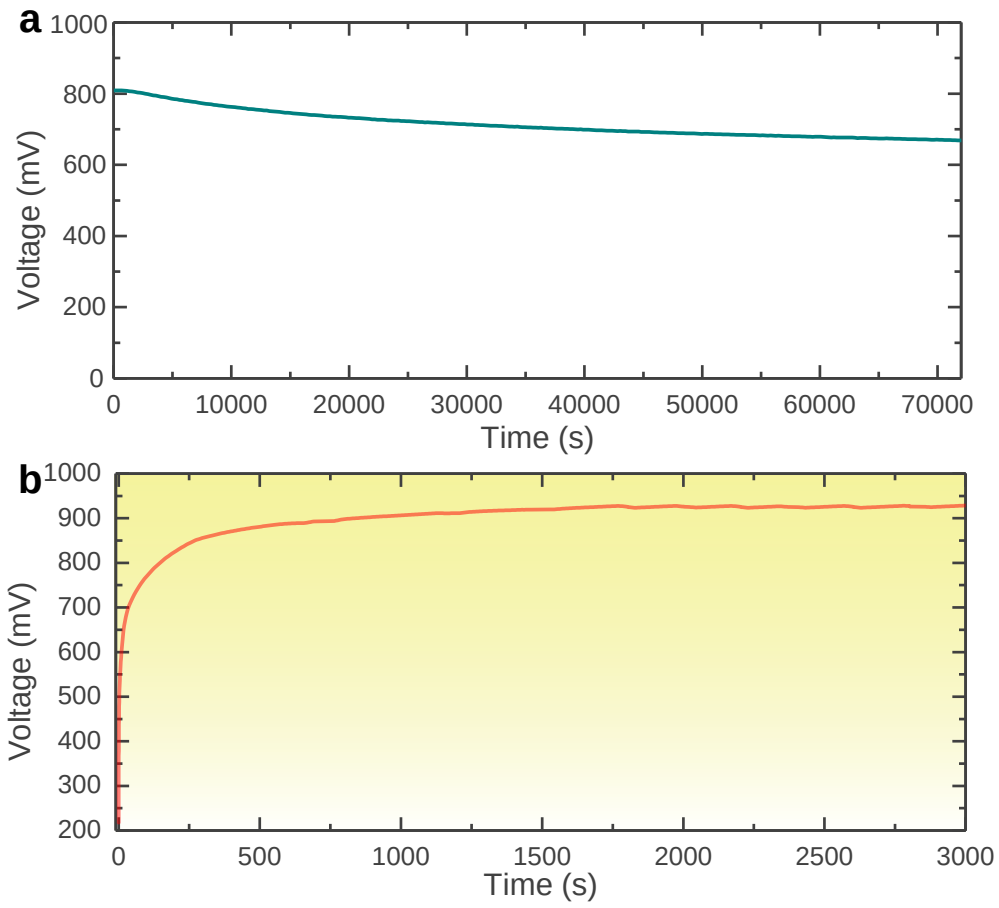

Figure S16. *(a) Self-discharge and (b) voltage floating test under continuous light illumination (λ ~ 420 nm, intensities of ~ 50 mWcm^{-2}) of the Photo-ZIC.*

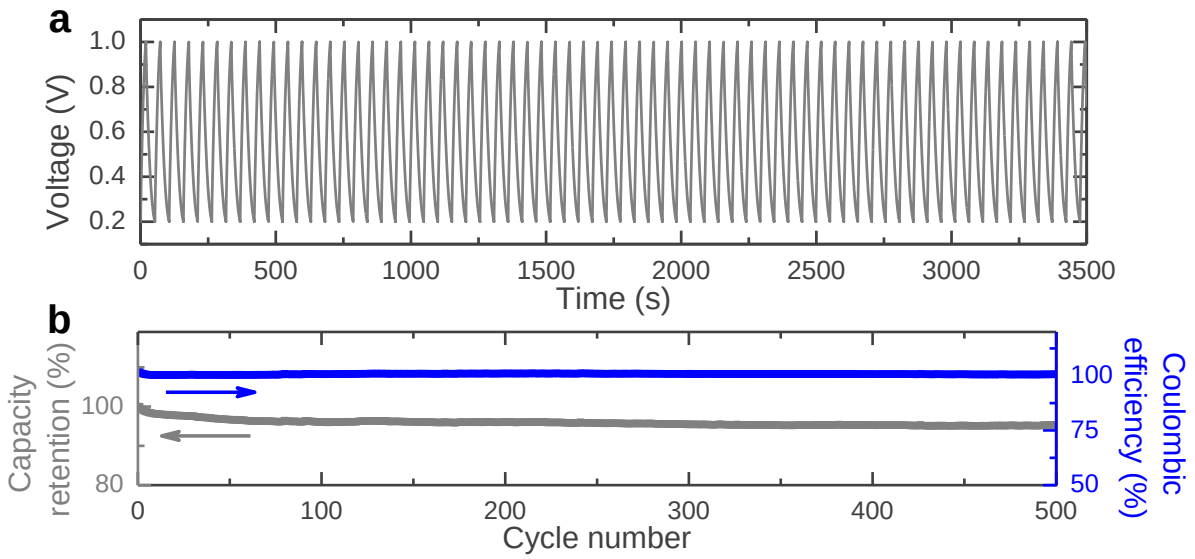

Figure S17. *Cyclic charge-discharge profile for 500 cycles of the Photo-ZIC at the specific current of 15 mAg^{-1}: (a) few charge-discharge cycles and (b) Capacity retention and coulombic efficiency plots. The Photo-ZIC retains ~ 95.3% capacity their capacity over 500 galvanostatic charge-discharge cycles.*

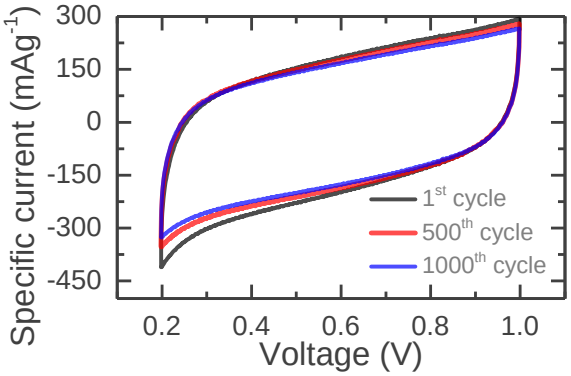

Figure S18. *Comparative 1st (black), 500th (red) and 1000th (blue) CV responses of the Photo-ZIC under illumination.*

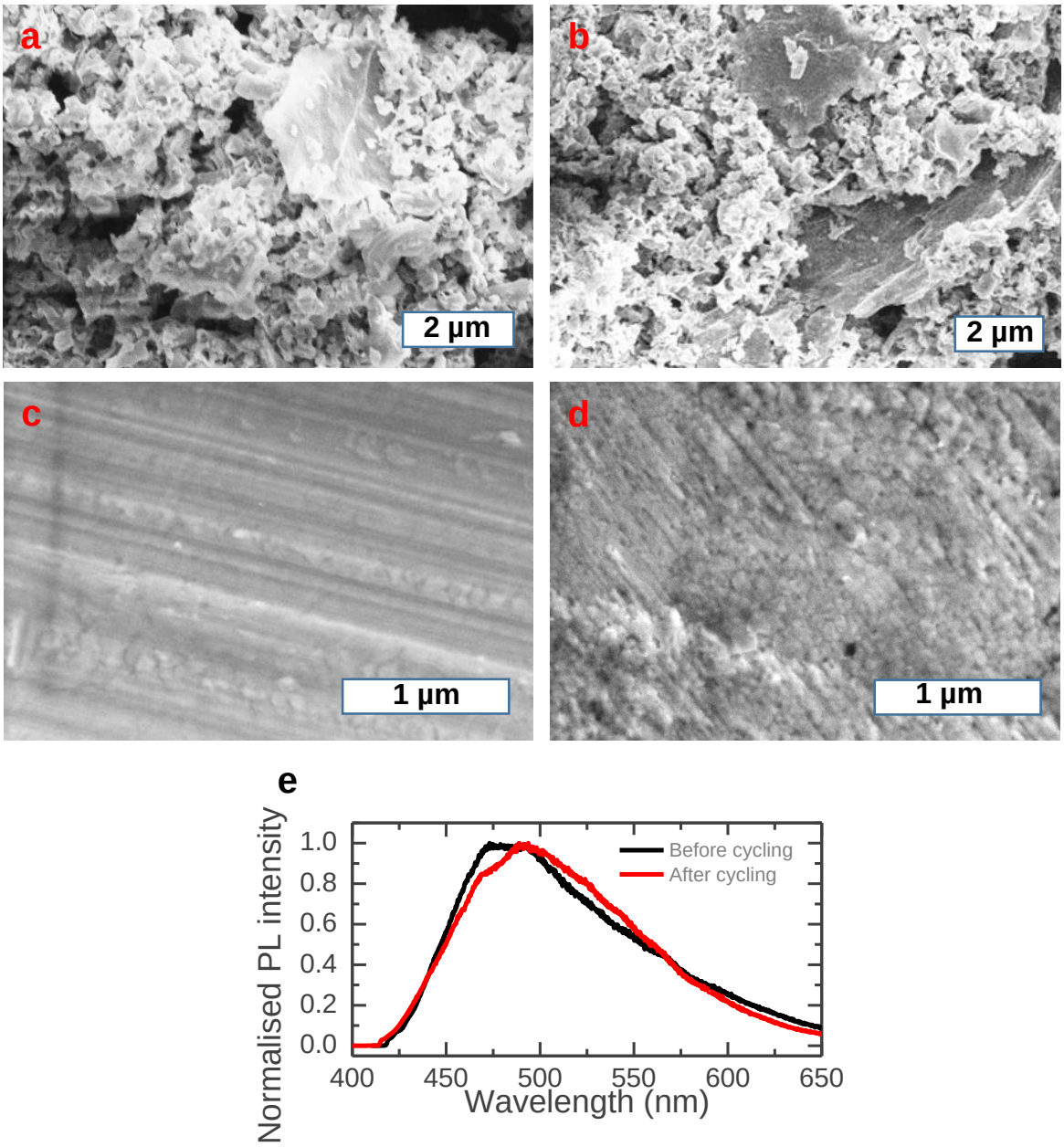

Figure S19. *SEM images of the (a,b) g-C_3N_4@rGO/FTO cathode and (c,d) Zn anode before and after 1000 CV cycles under illumination. (e) Normalised PL spectra of the g-C_3N_4@rGO/FTO cathode before (black) and after (red) 1000 CV cycles under illumination (λ ~ 420 nm, intensity ~ 50 mWcm^{-2}).*

Calculation:

The photo-charge conversion efficiency (η) can be expressed as[22],

$$\eta = \frac{E_{out}}{E_{in}} \times 100\% = \frac{E_m \times m}{P_{in} \times t \times A} \times 100\%$$

$$\eta = \frac{0.668\ (mW\ g^{-1}) \times 0.0002\ (g) \times 3600\ (s)}{50\ (mW\ cm^{-2}) \times 191\ (s) \times 0.5\ (cm^2)} \times 100\%$$

$$\eta \approx 0.01\ \%$$

where, E_m (= 668 mWhkg^{-1}) and m (= 0.2 mg) are the energy density and electrode mass of the photo-ZIC respectively, P_{in} (= 50 mW cm^{-2}) is the illuminated light intensity, t (= 191 s) is the photo-charging time and A (= 0.5 cm^2) is the light illuminated active surface area.

References

1. Fina, F.; Callear, S. K.; Carins, G. M.; Irvine, J. T. S. Structural Investigation of Graphitic Carbon Nitride via XRD and Neutron Diffraction. *Chem. Mater.* **2015**, *27*, 2612-2618.

2. Xue, J.; Ma, S.; Zhou, Y.; Zhang, Z.; He, M. Facile Photochemical Synthesis of Au/Pt/g-C3N4 with Plasmon-Enhanced Photocatalytic Activity for Antibiotic Degradation, *ACS Appl. Mater. Interfaces* **2015**, *7*, 9630-9637.

3. Yan, S. C.; Li, Z. S.; Zou, Z. G. Photodegradation Performance of g-C3N4 Fabricated by Directly Heating Melamine. *Langmuir* **2009**, *25*, 10397-10401.

4. Chen, X.; Kuo, D. H.; Lu, D. Nanonization of g-C3N4 with the assistance of activated carbon for improved visible light photocatalysis, *RSC Adv.* **2016**, *6*, 66814-66821.

5. Xiang, Q.; Yu, J.; Jaroniec, M. Preparation and Enhanced Visible-Light Photocatalytic H2-Production Activity of Graphene/C3N4 Composites. *J. Phys. Chem. C* **2011**, *115*, 7355-4363.

6. Lyth, S. M.; Nabae, Y.; Moriya, S.; Kuroki, S.; Kakimoto, M. A.; Ozaki, J. I.; Miyata, S. Carbon Nitride as a Nonprecious Catalyst for Electrochemical Oxygen Reduction. *J. Phys. Chem. C* **2009**, *113*, 20148-20151.

7. Miyasaka, T.; Murakami, T. N. The photocapacitor: An efficient self-charging capacitor for direct storage of solar energy. *Appl. Phys. Lett.* **2004**, *85*, 3932.

8. Chen, H. W.; Hsu, C. Y.; Chen, J. G.; Lee, K. M.; Wang, C. C.; Huang, K. C.; Ho, K. C. Plastic dye-sensitized photo-supercapacitor using electrophoretic deposition and compression methods. *J. Power Sources* **2010**, *195*, 6225-6231.

9. Chen, T.; Qiu, L. B.; Yang, Z. B.; Cai, Z. B.; Ren, J.; Li, H. P.; Lin, H. J.; Sun, X. M.; Peng, H. S. An Integrated "energy wire" for both photoelectric conversion and energy storage. *Angew. Chem. Int. Ed.* **2012**, *51*, 11977-11980.

10. Zhou, F.; Ren, Z.; Zhao, Y.; Shen, X.; Wang, A.; Li, Y. Y.; Surya, C.; Chai, Y. Perovskite Photovoltachromic Supercapacitor with All-Transparent Electrodes. *ACS Nano* **2016**, *10*, 5900-5908.

11. Xu, X.; Li, S.; Zhang, H.; Shen, Y.; Zakeeruddin, S. M.; Graetzel, M.; Cheng, Y. B.; Wang, M. A Power Pack Based on Organometallic Perovskite Solar Cell and Supercapacitor. *ACS Nano* **2015**, *9*, 1782-1787.

12. Yang, Z.; Deng, J.; Sun, H.; Ren, J.; Pan, S.; Peng, H. Self-Powered Energy Fiber: Energy Conversion in the Sheath and Storage in the Core. *Adv. Mater.* **2014**, *26*, 7038-7042.

13. Chen, X.; Sun, H.; Yang, Z.; Guan, G.; Zhang, Z.; Qiu, L.; Peng, H. A novel “energy fiber” by coaxially integrating dye-sensitized solar cell and electrochemical capacitor. *J. Mater. Chem. A* **2014**, *2*, 1897-1902.

14. Xu, J.; Wu, H.; Lu, L.; Leung, S. F.; Chen, D.; Chen, X.; Fan, Z.; Shen, G.; Li, D. Integrated Photo-supercapacitor Based on Bi-polar TiO2 Nanotube Arrays with Selective One-Side Plasma-Assisted Hydrogenation. *Adv. Funct. Mater.* **2014**, *24*, 1840-1846.

15. Fu, Y.; Wu, H.; Ye, S.; Cai, X.; Yu, X.; Hou, S.; Kafafy, H.; Zou, D. Integrated power fiber for energy conversion and storage. *Energy Environ. Sci.* **2013**, *6*, 805-812.

16. Cohn, A. P.; Erwin, W. R.; Share, K.; Oakes, L.; Westover, A. S.; Carter, R. E.; Bardhan, R.; Pint, C. L. All Silicon Electrode Photocapacitor for Integrated Energy Storage and Conversion. *Nano Lett.* **2015**, *15*, 2727-2731.

17. Zhang, Z. T.; Chen, X. L.; Chen, P. N.; Guan, G. Z.; Qiu, L. B.; Lin, H. J.; Yang, Z. B.; Bai, W. Y.; Luo, Y. F.; Peng, H. S. Integrated polymer solar cell and electrochemical supercapacitor in a flexible and stable fiber format. *Adv. Mater.* **2014**, *26*, 466-470.

18. Xu, J.; Ku, Z.; Zhang, Y.; Chao, D.; Fan, H. J. Integrated Photo-Supercapacitor Based on PEDOT Modified Printable Perovskite Solar Cell. *Adv. Mater. Technol.* **2016**, *1*, 1600074.

19. Liang, J.; Zhu, G.; Lu, Z.; Zhao, P.; Wang, C.; Ma, Y.; Xu, Z.; Wang, Y.; Hu, Y.; Ma, L.; Chen, T. Integrated perovskite solar capacitors with high energy conversion efficiency and fast photo-charging rate. *J. Mater. Chem. A* **2018**, *6*, 2047-2052.

20. Liang, J.; Zhu, G.; Wang, C.; Wang, Y.; Zhu, H.; Hu, Y.; Lv, H.; Chen, R.; Ma, L.; Chen, T.; Jin, Z.; Liu, J. MoS2-Based All-Purpose Fibrous Electrode and Self-Powering Energy Fiber for Efficient Energy Harvesting and Storage. *Adv. Energy Mater.* **2016**, 7, 601208.

21. Liang, J.; Zhu, G.; Lu, Z.; Zhao, P.; Wang, C.; Ma, Y.; Xu, Z.; Wang, Y.; Hu, Y.; Ma, L; Chen, T. Integrated perovskite solar capacitors with high energy conversion efficiency and fast photo-charging rate. *J. Mater. Chem. A* **2018**, *6*, 2047-2052.

22. Liu, R.; Wang, J.; Sun, T.; Wang, M.; Wu, C.; Zou, H.; Song, T.; Zhang, X.; Lee, S. T.; Wang, Z. L.; Sun, B. Silicon nanowire/polymer hybrid solar cell-supercapacitor: a self-charging power unit with a total efficiency of 10.5%. *Nano Lett.* **2017**, *17*, 4240-4247.